Rydberg Platform for Nonergodic Chiral Quantum Dynamics

Riccardo J. Valencia-Tortora,[1,*] Nicola Pancotti,[2] Michael Fleischhauer,[3] Hannes Bernien,[4] and Jamir Marino[1]
[1]Institut für Physik, Johannes Gutenberg-Universität Mainz, D-55099 Mainz, Germany
[2]AWS Center for Quantum Computing, Pasadena, California 91125, USA
[3]Department of Physics and Research Center OPTIMAS, University of Kaiserslautern-Landau, D-67663 Kaiserslautern, Germany
[4]Pritzker School of Molecular Engineering, University of Chicago, Chicago, Illinois 60637, USA

(Received 25 October 2023; revised 16 February 2024; accepted 15 April 2024; published 29 May 2024)

We propose a mechanism for engineering chiral interactions in Rydberg atoms via a *directional* antiblockade condition, where an atom can change its state only if an atom to its right (or left) is excited. The scalability of our scheme enables us to explore the many-body dynamics of kinetically constrained models with unidirectional character. We observe nonergodic behavior via either scars, confinement, or localization, upon simply tuning the strength of two driving fields acting on the atoms. We discuss how our mechanism persists in the presence of classical noise and how the degree of chirality in the interactions can be tuned, opening towards the frontier of directional, strongly correlated, quantum mechanics using neutral atoms arrays.

DOI: 10.1103/PhysRevLett.132.223201

Introduction.—Despite being far from full fault-tolerant quantum computing [1], reliable analog quantum simulations are nowadays attainable across a variety of atomic, molecular optical (AMO) as well as solid-state platforms. Among the former, atomic Rydberg arrays stand out prominently due to their remarkable degree of programmability, as highlighted in various studies [2–6]. This has led to groundbreaking experiments in areas such as topological order [7,8], engineerable quantum phase transitions [2,3,9,10], lattice gauge theories [11], and strongly correlated quantum dynamics [2,12–14]. Such broad flexibility suggests opportunities for designing quantum simulators with no direct counterpart in traditional AMO or condensed matter physics. In this context, a challenge centers on creating systems hosting nonreciprocal processes that can differentiate, particularly in one dimension, between the flow of information in the right and left directions. Directionality, already when restricted to *single-particle* processes, has proven useful in various tasks, such as mitigating backaction effects [15], realizing chiral transport [16], aiding the preparation of nontrivial topological states [17–20], and realizing unconventional phases of matter [21,22]. Thus, combining directional *interactions* with the high control achieved in Rydberg platforms would pave the way for entering the realm of chiral *strongly correlated* phenomena as an uncharted frontier of quantum information processing [23].

In this work, we achieve this goal by presenting a blueprint for Rydberg atomic arrays featuring chiral interactions that are not symmetric when neighboring atoms are exchanged. Specifically, we consider a one-dimensional array with a staggered configuration of atomic positions and drive fields [cf. Fig. 1(a)]. In such a scenario, due to strong Van der Waals interactions, we can access a regime we term *directional* antiblockade, wherein an atom can change its internal state solely when an atom to its right (or left) becomes excited. We then show the robustness of these mechanisms to experimental imperfections, like thermal disorder in atomic positions, opening up its usage in state-of-the-art platforms and for simulating exotic many-body systems, such as directional kinetically constrained quantum models (KCMs). KCMs have attracted considerable interest due to their capability to display nonergodic behavior despite their nonintegrable and disorder-free character [22,24–29]. In KCMs, slowdown of thermalization could occur through various mechanisms: quantum scars [2,30–35], realized in Rydberg arrays [2] or with superconducting qubits [36], where a few nonthermal excited states can lead to non-relaxing dynamics; Hilbert space shattering [37], realized in ultracold atoms [38,39]; confinement of quasi-particles induced by many-body interactions [11,40–42], observed in trapped ions [43]; or slow dynamics resulting from localization [24,25]. These mechanisms are intricately linked to the specific constraints at play, and each of them would necessitate a distinct experimental platform. Remarkably, in our Rydberg implementation, we can realize all of these mechanisms by simply adjusting the strength of the external drive fields. This versatility transforms our platform into a universal quantum simulator for nonergodic quantum dynamics. As an additional benefit, our platform allows for the implementation of the quantum East model [24,44], which has been absent in prior studies, albeit several Rydberg implementations have focused on related constrained models [45–51]. The significance of the quantum East model lies in its distinction as one of the rare cases where an interacting system undergoes a disorder-free transition between

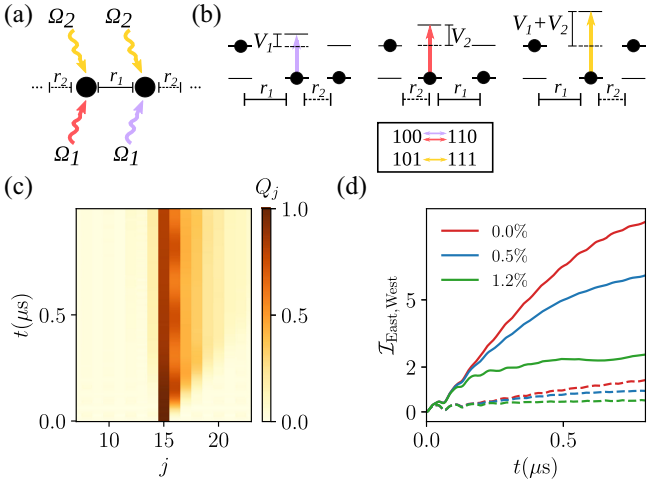

FIG. 1. (a) An array of Rydberg atoms in a staggered configuration of drive fields (each color refers to a different frequency) and spacings r_1 and r_2, with corresponding nearest-neighbor interactions V_1 and V_2. (b) Scheme of the most resonant processes (see box) that happen exclusively at the right of excited atoms due to the *directional* antiblockade. (c) Dynamics of the excitation profile seeding a single excitation for experimentally feasible parameters, including thermal disorder in the atomic positions $\tilde{\eta}_x = 0.012$ (see text). (d) Dynamics of the imbalances $\mathcal{I}_{\mathrm{East}}$ (continuous line) and $\mathcal{I}_{\mathrm{West}}$ (dashed line) starting from the same state as in (c) for different $\tilde{\eta}_x$. The imbalance $\mathcal{I}_{\mathrm{East}}$ ($\mathcal{I}_{\mathrm{West}}$) is given by the sum of the excitations to the right (left) of the initially seeded one. Excitations propagate preferably towards East as desired ($\mathcal{I}_{\mathrm{East}} > \mathcal{I}_{\mathrm{West}}$) despite finite temperature effects.

delocalization and localization in the ground state and dynamics [24], in a fashion markedly distinct from many-body localization [52,53].

Chiral interactions in Rydberg arrays.—The key ingredient to engineer a directional interaction is a staggered configuration of the atomic spacings and drive fields in a Rydberg array [cf. Fig. 1(a)]. The Hamiltonian describing such a scenario, in the rotating frame with respect to the bare atomic transitions, can be written as

$$\hat{H}(t) = V_1 \sum_{j\,\mathrm{odd}} \hat{Q}_j \hat{Q}_{j+1} + V_2 \sum_{j\,\mathrm{even}} \hat{Q}_j \hat{Q}_{j+1} + V_{\mathrm{NNN}} \sum_{j=1}^{N-2} \hat{Q}_j \hat{Q}_{j+2} + \frac{1}{2} \sum_{j=1}^{N} (\Omega_j(t) \hat{\sigma}_j^+ + \mathrm{H.c.}), \quad (1)$$

where $\hat{\sigma}_j^+ = |1\rangle_{jj}\langle 0|$ transfers the jth atom from the ground state $|0\rangle$ to the Rydberg state $|1\rangle$; $\hat{Q}_j = |1\rangle_{jj}\langle 1|$; V_1 (V_2) are Van der Waals interactions [$V(r) = C_6/r^6$] on odd (even) bonds; V_{NNN} is the next-nearest neighbor interaction; $\Omega_j(t) = \Omega_1 e^{-iV_{j-1,j}t} + \Omega_2 e^{-i(V_1+V_2)t}$ a classical drive field with $V_{j-1,j}$ the Van der Waals interaction on the $(j-1)$th bond, and $\Omega_{1,2}$ independent Rabi frequencies. Throughout, we work in the regime $V_{1,2}, |V_1 - V_2| \gg \Omega_{1,2} \gg V_{\mathrm{NNN}}$. In this regime, interactions play a crucial role in dictating the dynamics of the single atom. Specifically, two extreme scenarios can be realized: excited atoms either inhibit spin flips of neighboring ones (blockade) [54], or facilitate them (antiblockade) [55]. The blockade condition occurs by setting the drive field resonant with the bare atomic transitions so that the interaction energy due to a neighboring excited atom makes it off resonant. Instead, the antiblockade occurs when the acting drive field is detuned from the bare atomic transitions by the interaction, and thus it becomes resonant solely if a neighboring atom is excited. In translational invariant systems, each atom cannot distinguish its right neighbor from the one to its left, and so no preferable direction can appear. In our scheme instead, since $V_1 \neq V_2$, the atom can distinguish the two neighboring atoms and we can selectively make processes resonant towards one direction and off-resonance towards the other. We term this mechanism *directional* antiblockade, which implies that an atom can flip only when an atom to its right (or left) is excited. To achieve this regime, it is enough to apply the drive field controlled by Ω_1 on each atom, and so we temporarily set $\Omega_2 = 0$. The drive field $\Omega_1 e^{-iV_{j-1,j}t}$ acting on site j is detuned by V_1 (if j is even) or V_2 (if j is odd) from the bare atomic transition, so that it is resonant solely when the atom to its left is excited and the one to its right is not, obtaining the anticipated *directional* antiblockade [see Fig. 1(b)]. The net result is that an excitation seeded in the system triggers an avalanche of excitations solely toward "East" [see Fig. 1(c)]. In the Supplemental Material [56], we give further details on the experimental setup, and an alternative scheme where the staggered configuration is imprinted on the atomic frequencies while the drive field is monochromatic.

Experimental realization.—In actual experiments, the *directional* antiblockade could be spoiled by finite temperature fluctuations, inhomogeneities due to the harmonic frequency trap holding the atoms, or dephasing coming from finite laser linewidth. The first two can be taken into account including quenched disorder in the atomic positions [61]. Specifically, at low enough temperature T, the displacements $\delta\mathbf{r}_j$ from the ideal atomic positions are constant during a single experimental realization and distributed accordingly to a Gaussian distribution with zero average and width $\eta_\alpha = \sqrt{k_B T/(m\omega_\alpha^2)}$ along the α axis, with ω_α the trapping frequency and m the atomic mass. Instead, dephasing induced by finite linewidth of the laser can be modeled by a Lindblad master equation with jump operators $\hat{L}_j = \sqrt{\gamma}\hat{Q}_j$, with $j \in [1, N]$. Yet, in our setup, we work in regimes where $\gamma \sim 10$ kHz is at least 2 orders of magnitudes smaller than the other energy scales, and therefore it can be neglected. Specifically, we will show results up to a time of 10 μs, where our approximations hold and spontaneous decay from the Rydberg state can be neglected. We elaborate further in the conclusions and [56] on the opposite limit, where dephasing is large, illustrating how our scheme readily enables us to investigate "classical"

dynamics with directional character. For concreteness, we consider ^{87}Rb atoms located along the x axis, at temperature $T = 3$ μK and optical traps with $\omega_x = \omega_y = 5 \times \omega_z = 40$ kHz, which give rise to an anisotropic disorder $\eta_x = \eta_y = \eta_z/5 \approx 0.1$ μm. We consider the atomic level $70S$ as the Rydberg state which has $C_6/(2\pi) = 864$ GHz/(μm)^6. In the following, we measure disorder as the relative variation with respect to the mean distance, namely, $\tilde{\eta}_\alpha \equiv \eta_\alpha/r_1$. We consider Rabi frequencies $\Omega_{1,2}$ in the range between $2\pi \times 1$ MHz and $2\pi \times 5$ MHz. For this set of parameters, we found $V_1/(2\pi) = (15.0 \pm 1.0)$ MHz, $V_2/(2\pi) = (30.0 \pm 2.2)$ MHz, and $V_{\mathrm{NNN}}/(2\pi) = (0.33 \pm 0.02)$ MHz, as a good compromise between fast dynamics, small impact of disorder, and $\Omega_{1,2} \ll \{V_{1,2}, |V_1 - V_2|\}$. In the experiment, these interactions correspond to average spacings $r_1 = 6.2$ μm and $r_2 = 5.4$ μm, for which $\tilde{\eta}_x \approx 0.01$. Despite we show results mostly in this parameters' regime, we keep $\tilde{\eta}_\alpha$ as a free parameter to explore different experimental scenarios. In the following, we show results averaged over 50 realizations of disorder, for which statistical errors are ∼1% or less. As can be seen in Figs. 1(c)–1(d), the main impact of disorder is a reduction of the propagating front, while its directional character is not appreciably spoiled. Having shown the robustness of our scheme, we now proceed to discuss some models immediately accessible by simply tuning the strength of the external drive fields.

Kinetically constrained models.—Before discussing the resulting dynamics of our scheme, we note that using a single drive field, an atom remains frozen when both neighbors are excited. To enrich dynamics, we reintroduce the additional global drive field with frequency detuned by $V_1 + V_2$ from the bare atomic transition, i.e., $\Omega_2 e^{-i(V_1+V_2)t}$, so that it allows the transition $|101\rangle \leftrightarrow |111\rangle$ [cf. Fig. 1(b)] [56]. As is apparent, there is still no resonant process where an atom changes its state in the absence of an excited one to its left. To make it visible, we write down the following effective Hamiltonian describing the most resonant processes without taking into account disorder in the atomic positions (for further details see [56]):

$$\hat{H} = \frac{\Omega_1}{2}\sum_j \hat{Q}_j \hat{X}_{j+1} \hat{P}_{j+2} + \frac{\Omega_2}{2}\sum_j \hat{Q}_j \hat{X}_{j+1} \hat{Q}_{j+2} + \epsilon \sum_j \hat{Q}_j + V_{\mathrm{NNN}} \sum_j \hat{Q}_j \hat{Q}_{j+2}, \tag{2}$$

where $\hat{X} = |0\rangle\langle 1| + |1\rangle\langle 0|$, $\hat{P} = 1 - \hat{Q}$, and we have introduced the detuning ϵ from the perfect *directional* anti-blockade which, together with V_{NNN}, can spoil the perfect resonance condition and inhibit spin flips, as we will show later. The Hamiltonian in Eq. (2) belongs to the family of kinetically constrained quantum East models, where dynamics are activated solely to the right of excited sites. East models are characterized by a so-called "East symmetry" [24], which implies that empty regions without excitations to their left remain frozen. As a consequence, the location of the first excitation encountered starting from the left edge of the system does not change [see Fig. 1(c)], and the Hilbert space splits in N disconnected sectors, with N the system size. Once the East symmetry sector is specified by the location of the first excitation, we can further shape the accessible Hilbert space simply by changing the relative power of the drive fields Ω_1 and Ω_2 [cf. Fig. 2(a)], which directly reflects in the mobility of excitations. Specifically, we will show that with a single drive field the East symmetry sector *shatters* in $\mathcal{O}(e^N)$ disconnected sectors [62], while when both are active it is irreducible [24], meaning the dynamics connect all states (see Fig. 2). Then, we will illustrate the mechanisms by which in each regime the onset of thermalization considerably slows down within each irreducible sector, exhibiting scars, confinement, and localization (in [56] we provide further details on the dynamical features in each regime). In the following, we discuss these three regimes using the effective Hamiltonian in Eq. (2) as guidance. Then, we

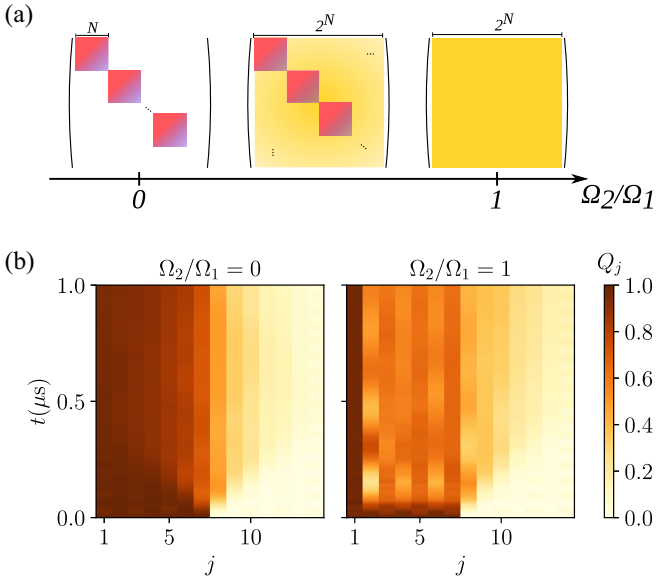

FIG. 2. (a) Sketch of the accessible Hilbert space upon initializing product states, at fixed East symmetry sector, in a system of size N as a function of the Rabi frequencies $\Omega_{1,2}$. Colors indicate allowed transitions and they are in one-to-one correspondence with those used for the drive fields in Fig. 1(a). Blank spaces indicate forbidden transitions. For $\Omega_1 \neq 0$ and $\Omega_2 = 0$ strings of excitations can only shrink or expand without merging or splitting, leading to Hilbert space *shattering*; for $\Omega_2/\Omega_1 \neq 0$, strings achieve complete mobility, rendering the system ergodic, as any product state becomes accessible from any other. For $\Omega_2/\Omega_1 = 1$ we recover the quantum East model [24,44]. (b) Dynamics of the excitation profile starting from the product state $\otimes_{j=1}^{N/2} |1\rangle \otimes_{j=N/2+1}^{N} |0\rangle$ in the shattered ($\Omega_2 = 0$) and ergodic regime ($\Omega_{1,2} \neq 0$) including thermal disorder $\tilde{\eta}_x = 0.012$ in units of the average spacing $r_1 = 6.2$ μm.

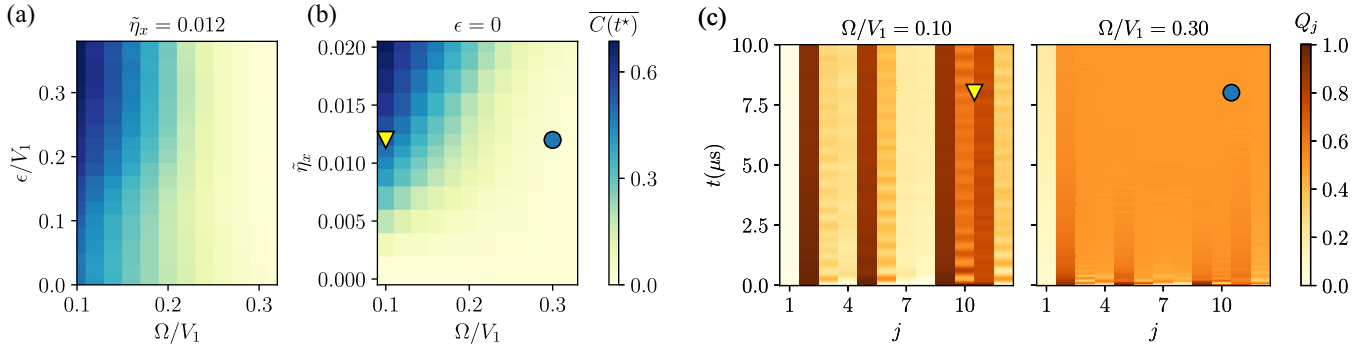

FIG. 3. Dynamics of the state $|010010001110\rangle$ under the full theory [cf. Eq. (1)] in the quantum East model regime ($\Omega_{1,2} = \Omega$). (a)–(b) Time-averaged autocorrelation function [cf. Eq. (4)] $\overline{C(t^\star)}$ at time $t^\star = 10$ μs keeping fixed either thermal disorder $\tilde{\eta}_x$ or detuning ϵ, respectively. For small Ω the memory of the initial state is kept up to long times [$\overline{C(t^\star)} > 0$], while instead for large Ω the memory of the initial state is rapidly washed out [$\overline{C(t^\star)} \approx 0$]. (c) Dynamics of the excitation profile in the two phases [marked via symbols in (b)] at fixed thermal disorder $\tilde{\eta}_x = 0.012$ in units of the average spacing $r_1 = 6.2$ μm (see text).

show how those features survive upon simulating the full theory in Eq. (1).

QXQ model.—For $\Omega_1 = 0$ and $\Omega_2 \neq 0$ directionality is lost and a spin flip occurs solely when both neighboring atoms are excited. This is reminiscent of the well-known PXP model, in which a spin flip occurs when both neighboring atoms are in the ground state. Indeed, the PXP model and ours share the same physics as they are connected via the transformation $\hat{U} = \prod_{j=1}^{N} \hat{X}_j$, which translates to interchanging $|0\rangle \leftrightarrow |1\rangle$. This includes Hilbert space *shattering* [63] and the presence of quantum many-body scars, which slow down the onset of thermalization when initializing specific states (e.g., Néel state) [2,31].

QXP model.—When $\Omega_1 \neq 0$ and $\Omega_2 = 0$, strings of consecutive excitations can shrink or grow but not merge or split ($|101\rangle \not\leftrightarrow |111\rangle$), effectively experiencing a repulsive interaction. Additionally, the unidirectional character of the dynamics further reduces their mobility since the left edge of each string cannot move. Because of these constraints, each string of excitations is confined between its left edge and the left edge of the next one, and no entanglement can be generated between them during dynamics. As a result, the Hilbert space gets shattered in $\mathcal{O}(e^N)$ disconnected sectors [62]. Since each string of excitations evolves independently from the others, we will focus on the largest irreducible sector containing a single string. We find that its dynamics (for $\epsilon = 0$) are described by the Hamiltonian [56]

$$\hat{H} = \frac{\Omega_1}{2} \sum_{k=1}^{N-1} (|\boldsymbol{k}\rangle\langle \boldsymbol{k}+\boldsymbol{1}| + \text{H.c.}) + V_{\text{NNN}} \sum_{k=2}^{N} (k-2)|\boldsymbol{k}\rangle\langle \boldsymbol{k}|, \quad (3)$$

with $|\boldsymbol{k}\rangle \equiv |1\rangle^k |0\rangle^{N-k}$, where the first term controls the change of the string length, while the second the potential energy proportional to its length. This Hamiltonian is integrable and has been derived in similar scenarios [42,64–66]. Direct inspection shows that Eq. (3) is the well-known Hamiltonian of an electron in a lattice subjected to a constant electric field [65,66]. Dynamics display Stark localization [65], which leads to real-time Bloch oscillations of period $T_{\text{Bloch}} = 2\pi\Omega_1/V_{\text{NNN}}$ and size $\ell_{\text{Bloch}} \sim \Omega_1/V_{\text{NNN}}$ originating from the rightmost edge of the string. Hence, excitations and quantum correlations are confined, preventing thermalization, closely resembling confinement in nonintegrable systems [11,40,41,67]. Upon introducing disorder, Bloch oscillations are still visible [see Fig. 2(b) and [56]] although partly suppressed.

Quantum East model.—When both drive fields are active ($\Omega_{1,2} \neq 0$), strings of excitations gain full mobility since they can shrink, grow, merge, and split [cf. Fig. 2(b)]. Thus, the accessible Hilbert space does not shatter and any product state can be dynamically reached by any other at fixed East symmetry sector [24]. Nonetheless, it is still possible to observe an extreme slowdown of thermalization. This can be immediately seen by setting $\Omega_2/\Omega_1 = 1$, for which Eq. (2) reduces to the quantum East model investigated in Refs. [24,44] apart from additional density-density interactions, which do not alter the qualitative picture. This model has been shown to display a dynamical transition separating a fast and slow thermalizing phase [24,44] due to the competing kinetic term $\propto \Omega$ and on-site energy $\propto \epsilon$. Intuitively, if the kinetic term dominates ($\Omega_{1,2}/(2\epsilon) \gtrsim 1$) strings of excitations expand and merge ballistically, quickly washing local information of the initial configuration, while if it is subleading ($\Omega_{1,2}/(2\epsilon) \lesssim 1$), excitations expand slowly, making it possible to retrieve information about the initial conditions. Such behavior is strongly linked to the localization of the ground state and it can be observed for an exponentially large number, in the system size, of initial states [24]. Upon introducing thermal disorder $\tilde{\eta}_\alpha$, the picture is slightly affected. Indeed, $\tilde{\eta}_\alpha$ can already induce undesired mismatches from the perfect resonant *directional* antiblockade

condition and aid localization. Thus, we expect the dynamics to be dictated by the competition of Ω and the joint contribution of $\tilde{\eta}_\alpha$ and ϵ. We test this by initializing a representative high-temperature product state characterized by regions with low and high densities of excitations. In the slow phase, heterogeneity in the initial state plays a crucial role in dictating the dynamics up to very long times, in contrast with typical fast thermalizing systems where all local information is quickly lost except for global conserved quantities. We choose the autocorrelation function [22,24]

$$C(t) = \frac{2}{Z}\sum_i \langle \hat{Q}_i(t)\hat{Q}_i(0)\rangle - 1, \tag{4}$$

where $Z = \sum_i \langle \hat{Q}_i(0)\rangle$ is a normalization constant, as proxy for distinguishing the different dynamical phases. For the initial product state considered, $C(t)$ is the density of the initially excited sites at time t, to which we subtract an evenly distributed "background" corresponding to an infinite temperature state with $\langle \hat{Q}_i\rangle = 1/2$. Thus, $C(t)$ serves as a good proxy for the memory of initial conditions, as its initial value is $C(t=0) = 1$ and tends to zero when the system thermalizes. In Figs. 3(a) and 3(b) we show the time average $\overline{C(t^\star)} = \int_0^{t^\star} C(\tau)d\tau/t^\star$ up to experimentally accessible time windows using the full theory [cf. Eq. (1)] in two scenarios: either keeping fixed the thermal disorder and varying ϵ, or vice versa. As anticipated, both ϵ and $\tilde{\eta}_\alpha$ contribute to slowing down dynamics. Indeed, in both dynamical phase diagrams, we can distinguish a phase where the system retains memory of the initial state and a phase where the system quickly thermalizes and all local memory is quickly erased.

Perspectives.—In this work, we have proposed a scheme for realizing chiral interactions through a *directional* anti-blockade condition, namely an atom can change its internal state only if the atom to its right (or left) is excited. Our scheme is based on "energetic" arguments and gives rise to constrained interactions. Additionally, our protocol could be readily extended in the presence of dominant classical noise. In this regime, dynamics is effectively described by rate equations, with rates dependent on the detunings, interactions, and atomic configuration [45,47], opening up to the simulation of dissipative unidirectional spin dynamics (for further details see [56]). Finally, we highlight that the degree of chirality in the interactions can be tuned by relaxing the condition $\Delta V \equiv |V_1 - V_2| \gg \Omega_{1,2}$. Specifically, for $0 < \Delta V/\Omega_{1,2} \lesssim 1$, dynamics still has a preferable direction, but there are near-resonant processes towards the other as well (similar to other Rydberg proposals [68,69]). This offers a path for accessing regimes with a tunable *bias* towards one direction or the other. As an extreme example, in the zero *bias* case ($\Delta V = 0$), and by setting $\Omega_1 = \Omega_2/2$, we can effectively simulate the quantum Fredrickson-Andersen model [70,71].

R. J. V. T. is grateful to O. Chelpanova and especially to M. Stefanini for useful discussions. This project has been supported by the Deutsche Forschungsgemeinschaft (DFG, German Research Foundation) through the Project ID 429529648-TRR 306 QuCoLiMa ("Quantum Cooperativity of Light and Matter"), and the Grant No. HADEQUAM-MA7003/3-1; by the Dynamics and Topology Center, funded by the State of Rhineland Palatinate. This material is based upon work supported by the U.S. Department of Energy, Office of Science, National Quantum Information Science Research Centers. The work of M. F. has been supported by the DFG (SFB TR 185), Project No. 277625399. Parts of this research were conducted using the Mogon supercomputer and/or advisory services offered by Johannes Gutenberg University Mainz, which is a member of the Alliance for High Performance Computing in Rhineland Palatinate (AHRP), and the Gauss Alliance e.V. We gratefully acknowledge the computing time granted on the Mogon supercomputer at Johannes Gutenberg University Mainz through the project "DysQCorr."

*Corresponding author: rvalenci@uni-mainz.de

[1] J. Preskill, Quantum computing in the NISQ era and beyond, Quantum **2**, 79 (2018).
[2] H. Bernien, S. Schwartz, A. Keesling, H. Levine, A. Omran, H. Pichler, S. Choi, A. S. Zibrov, M. Endres, M. Greiner, V. Vuletić, and M. D. Lukin, Probing many-body dynamics on a 51-atom quantum simulator, Nature (London) **551**, 579 (2017).
[3] P. Scholl, M. Schuler, H. J. Williams, A. A. Eberharter, D. Barredo, K.-N. Schymik, V. Lienhard, L.-P. Henry, T. C. Lang, T. Lahaye, A. M. Läuchli, and A. Browaeys, Quantum simulation of 2D antiferromagnets with hundreds of Rydberg atoms, Nature (London) **595**, 233 (2021).
[4] D. Bluvstein, A. Omran, H. Levine, A. Keesling, G. Semeghini, S. Ebadi, T. T. Wang, A. A. Michailidis, N. Maskara, W. W. Ho, S. Choi, M. Serbyn, M. Greiner, V. Vuletić, and M. D. Lukin, Controlling quantum many-body dynamics in driven Rydberg atom arrays, Science **371**, 1355 (2021).
[5] A. Browaeys and T. Lahaye, Many-body physics with individually controlled Rydberg atoms, Nat. Phys. **16**, 132 (2020).
[6] H. Labuhn, D. Barredo, S. Ravets, S. de Léséleuc, T. Macrì, T. Lahaye, and A. Browaeys, Tunable two-dimensional arrays of single Rydberg atoms for realizing quantum Ising models, Nature (London) **534**, 667 (2016).
[7] S. de Léséleuc, V. Lienhard, P. Scholl, D. Barredo, S. Weber, N. Lang, H. P. Büchler, T. Lahaye, and A. Browaeys, Observation of a symmetry-protected topological phase of interacting bosons with Rydberg atoms, Science **365**, 775 (2019).

[8] G. Semeghini, H. Levine, A. Keesling, S. Ebadi, T. T. Wang, D. Bluvstein, R. Verresen, H. Pichler, M. Kalinowski, R. Samajdar, A. Omran, S. Sachdev, A. Vishwanath, M. Greiner, V. Vuletić, and M. D. Lukin, Probing topological spin liquids on a programmable quantum simulator, Science **374**, 1242 (2021).

[9] S. Ebadi, T. T. Wang, H. Levine, A. Keesling, G. Semeghini, A. Omran, D. Bluvstein, R. Samajdar, H. Pichler, W. W. Ho, S. Choi, S. Sachdev, M. Greiner, V. Vuletić, and M. D. Lukin, Quantum phases of matter on a 256-atom programmable quantum simulator, Nature (London) **595**, 227 (2021).

[10] A. Keesling, A. Omran, H. Levine, H. Bernien, H. Pichler, S. Choi, R. Samajdar, S. Schwartz, P. Silvi, S. Sachdev, P. Zoller, M. Endres, M. Greiner, V. Vuletić, and M. D. Lukin, Quantum Kibble-Zurek mechanism and critical dynamics on a programmable Rydberg simulator, Nature (London) **568**, 207 (2019).

[11] F. M. Surace, P. P. Mazza, G. Giudici, A. Lerose, A. Gambassi, and M. Dalmonte, Lattice gauge theories and string dynamics in Rydberg atom quantum simulators, Phys. Rev. X **10**, 021041 (2020).

[12] V. Lienhard, S. de Léséleuc, D. Barredo, T. Lahaye, A. Browaeys, M. Schuler, L.-P. Henry, and A. M. Läuchli, Observing the space- and time-dependent growth of correlations in dynamically tuned synthetic Ising models with antiferromagnetic interactions, Phys. Rev. X **8**, 021070 (2018).

[13] E. Guardado-Sanchez, P. T. Brown, D. Mitra, T. Devakul, D. A. Huse, P. Schauß, and W. S. Bakr, Probing the quench dynamics of antiferromagnetic correlations in a 2D quantum Ising spin system, Phys. Rev. X **8**, 021069 (2018).

[14] H. Kim, Y. Park, K. Kim, H.-S. Sim, and J. Ahn, Detailed balance of thermalization dynamics in Rydberg-atom quantum simulators, Phys. Rev. Lett. **120**, 180502 (2018).

[15] A. Kamal, J. Clarke, and M. H. Devoret, Noiseless nonreciprocity in a parametric active device, Nat. Phys. **7**, 311 (2011).

[16] A. McDonald, T. Pereg-Barnea, and A. A. Clerk, Phase-dependent chiral transport and effective non-Hermitian dynamics in a bosonic Kitaev-Majorana chain, Phys. Rev. X **8**, 041031 (2018).

[17] P. Lodahl, S. Mahmoodian, S. Stobbe, A. Rauschenbeutel, P. Schneeweiss, J. Volz, H. Pichler, and P. Zoller, Chiral quantum optics, Nature (London) **541**, 473 (2017).

[18] A. Clerk, Introduction to quantum non-reciprocal interactions: From non-Hermitian Hamiltonians to quantum master equations and quantum feedforward schemes, SciPost Phys. Lect. Notes (2022), 10.21468/scipostphyslectnotes.44.

[19] H. Pichler, T. Ramos, A. J. Daley, and P. Zoller, Quantum optics of chiral spin networks, Phys. Rev. A **91**, 042116 (2015).

[20] X. Wang, T. Liu, A. F. Kockum, H.-R. Li, and F. Nori, Tunable chiral bound states with giant atoms, Phys. Rev. Lett. **126**, 043602 (2021).

[21] M. Fruchart, R. Hanai, P. B. Littlewood, and V. Vitelli, Non-reciprocal phase transitions, Nature (London) **592**, 363 (2021).

[22] J. P. Garrahan, Aspects of non-equilibrium in classical and quantum systems: Slow relaxation and glasses, dynamical large deviations, quantum non-ergodicity, and open quantum dynamics, Physica (Amsterdam) **504**, 130 (2018).

[23] S.-H. Wei, B. Jing, X.-Y. Zhang, J.-Y. Liao, C.-Z. Yuan, B.-Y. Fan, C. Lyu, D.-L. Zhou, Y. Wang, G.-W. Deng *et al.*, Towards real-world quantum networks: A review, Laser Photonics Rev. **16**, 2100219 (2022).

[24] N. Pancotti, G. Giudice, J. I. Cirac, J. P. Garrahan, and M. C. Bañuls, Quantum east model: Localization, nonthermal eigenstates, and slow dynamics, Phys. Rev. X **10**, 021051 (2020).

[25] R. J. Valencia-Tortora, N. Pancotti, and J. Marino, Kinetically constrained quantum dynamics in superconducting circuits, PRX Quantum **3**, 020346 (2022).

[26] J. P. Garrahan, R. L. Jack, V. Lecomte, E. Pitard, K. van Duijvendijk, and F. van Wijland, First-order dynamical phase transition in models of glasses: An approach based on ensembles of histories, J. Phys. A **42**, 075007 (2009).

[27] P. Chleboun, A. Faggionato, and F. Martinelli, Time scale separation in the low temperature east model: Rigorous results, J. Stat. Mech. 2013, L04001 (2013).

[28] Z. Lan, M. van Horssen, S. Powell, and J. P. Garrahan, Quantum slow relaxation and metastability due to dynamical constraints, Phys. Rev. Lett. **121**, 040603 (2018).

[29] L. Causer, I. Lesanovsky, M. C. Bañuls, and J. P. Garrahan, Dynamics and large deviation transitions of the Xor-Fredrickson-Andersen kinetically constrained model, Phys. Rev. E **102**, 052132 (2020).

[30] C. J. Turner, A. A. Michailidis, D. A. Abanin, M. Serbyn, and Z. Papić, Weak ergodicity breaking from quantum many-body scars, Nat. Phys. **14**, 745 (2018).

[31] S. Choi, C. J. Turner, H. Pichler, W. W. Ho, A. A. Michailidis, Z. Papić, M. Serbyn, M. D. Lukin, and D. A. Abanin, Emergent su(2) dynamics and perfect quantum many-body scars, Phys. Rev. Lett. **122**, 220603 (2019).

[32] M. Serbyn, D. A. Abanin, and Z. Papić, Quantum many-body scars and weak breaking of ergodicity, Nat. Phys. **17**, 675 (2021).

[33] C. J. Turner, A. A. Michailidis, D. A. Abanin, M. Serbyn, and Z. Papić, Quantum scarred eigenstates in a Rydberg atom chain: Entanglement, breakdown of thermalization, and stability to perturbations, Phys. Rev. B **98**, 155134 (2018).

[34] V. Khemani, C. R. Laumann, and A. Chandran, Signatures of integrability in the dynamics of Rydberg-blockaded chains, Phys. Rev. B **99**, 161101(R) (2019).

[35] C. J. Turner, J.-Y. Desaules, K. Bull, and Z. Papić, Correspondence principle for many-body scars in ultracold rydberg atoms, Phys. Rev. X **11**, 021021 (2021).

[36] P. Zhang, H. Dong, Y. Gao, L. Zhao, J. Hao, J.-Y. Desaules, Q. Guo, J. Chen, J. Deng, B. Liu *et al.*, Many-body Hilbert space scarring on a superconducting processor, Nat. Phys. **19**, 120 (2023).

[37] P. Sala, T. Rakovszky, R. Verresen, M. Knap, and F. Pollmann, Ergodicity breaking arising from Hilbert space fragmentation in dipole-conserving Hamiltonians, Phys. Rev. X **10**, 011047 (2020).

[38] T. Kohlert, S. Scherg, P. Sala, F. Pollmann, B. Hebbe Madhusudhana, I. Bloch, and M. Aidelsburger, Exploring the regime of fragmentation in strongly tilted Fermi-Hubbard chains, Phys. Rev. Lett. **130**, 010201 (2023).
[39] S. Scherg, T. Kohlert, P. Sala, F. Pollmann, B. H. Madhusudhana, I. Bloch, and M. Aidelsburger, Observing non-ergodicity due to kinetic constraints in tilted Fermi-Hubbard chains, Nat. Commun. **12**, 4490 (2021).
[40] M. Kormos, M. Collura, G. Takács, and P. Calabrese, Real-time confinement following a quantum quench to a non-integrable model, Nat. Phys. **13**, 246 (2017).
[41] A. Lerose, F. M. Surace, P. P. Mazza, G. Perfetto, M. Collura, and A. Gambassi, Quasilocalized dynamics from confinement of quantum excitations, Phys. Rev. B **102**, 041118(R) (2020).
[42] M. Magoni, P. P. Mazza, and I. Lesanovsky, Emergent Bloch oscillations in a kinetically constrained Rydberg spin lattice, Phys. Rev. Lett. **126**, 103002 (2021).
[43] W. L. Tan, P. Becker, F. Liu, G. Pagano, K. S. Collins, A. De, L. Feng, H. B. Kaplan, A. Kyprianidis, R. Lundgren, W. Morong, S. Whitsitt, A. V. Gorshkov, and C. Monroe, Domain-wall confinement and dynamics in a quantum simulator, Nat. Phys. **17**, 742 (2021).
[44] M. van Horssen, E. Levi, and J. P. Garrahan, Dynamics of many-body localization in a translation-invariant quantum glass model, Phys. Rev. B **92**, 100305(R) (2015).
[45] I. Lesanovsky and J. P. Garrahan, Kinetic constraints, hierarchical relaxation, and onset of glassiness in strongly interacting and dissipative Rydberg gases, Phys. Rev. Lett. **111**, 215305 (2013).
[46] C. Pérez-Espigares, I. Lesanovsky, J. P. Garrahan, and R. Gutiérrez, Glassy dynamics due to a trajectory phase transition in dissipative Rydberg gases, Phys. Rev. A **98**, 021804(R) (2018).
[47] M. M. Valado, C. Simonelli, M. D. Hoogerland, I. Lesanovsky, J. P. Garrahan, E. Arimondo, D. Ciampini, and O. Morsch, Experimental observation of controllable kinetic constraints in a cold atomic gas, Phys. Rev. A **93**, 040701(R) (2016).
[48] I. Lesanovsky and J. P. Garrahan, Out-of-equilibrium structures in strongly interacting Rydberg gases with dissipation, Phys. Rev. A **90**, 011603(R) (2014).
[49] D. Gribben, I. Lesanovsky, and R. Gutiérrez, Quench dynamics of a dissipative Rydberg gas in the classical and quantum regimes, Phys. Rev. A **97**, 011603(R) (2018).
[50] M. Ostmann, M. Marcuzzi, J. P. Garrahan, and I. Lesanovsky, Localization in spin chains with facilitation constraints and disordered interactions, Phys. Rev. A **99**, 060101(R) (2019).
[51] M. Marcuzzi, J. c. v. Minář, D. Barredo, S. de Léséleuc, H. Labuhn, T. Lahaye, A. Browaeys, E. Levi, and I. Lesanovsky, Facilitation dynamics and localization phenomena in Rydberg lattice gases with position disorder, Phys. Rev. Lett. **118**, 063606 (2017).
[52] R. Nandkishore and D. A. Huse, Many-body localization and thermalization in quantum statistical mechanics, Annu. Rev. Condens. Matter Phys. **6**, 15 (2015).
[53] D. A. Abanin, E. Altman, I. Bloch, and M. Serbyn, Colloquium: Many-body localization, thermalization, and entanglement, Rev. Mod. Phys. **91**, 021001 (2019).
[54] D. Jaksch, J. I. Cirac, P. Zoller, S. L. Rolston, R. Côté, and M. D. Lukin, Fast quantum gates for neutral atoms, Phys. Rev. Lett. **85**, 2208 (2000).
[55] C. Ates, T. Pohl, T. Pattard, and J. M. Rost, Many-body theory of excitation dynamics in an ultracold Rydberg gas, Phys. Rev. A **76**, 013413 (2007).
[56] See Supplemental Material at http://link.aps.org/supplemental/10.1103/PhysRevLett.132.223201 for the details about the numerical methods, experimental setting, derivation of the effective theories, dynamical features in the different regimes, and discussion on classical rate equations, which includes Refs. [57–60].
[57] C. Chen, G. Bornet, M. Bintz, G. Emperauger, L. Leclerc, V. S. Liu, P. Scholl, D. Barredo, J. Hauschild, S. Chatterjee, M. Schuler, A. M. Läuchli, M. P. Zaletel, T. Lahaye, N. Y. Yao, and A. Browaeys, Continuous symmetry breaking in a two-dimensional Rydberg array, Nature (London) **616**, 691 (2023).
[58] A. Omran, H. Levine, A. Keesling, G. Semeghini, T. T. Wang, S. Ebadi, H. Bernien, A. S. Zibrov, H. Pichler, S. Choi, J. Cui, M. Rossignolo, P. Rembold, S. Montangero, T. Calarco, M. Endres, M. Greiner, V. Vuletić, and M. D. Lukin, Generation and manipulation of Schrödinger cat states in Rydberg atom arrays, Science **365**, 570 (2019).
[59] M. Fishman, S. R. White, and E. M. Stoudenmire, The ITensor software library for tensor network calculations, SciPost Phys. Codebases, 4 (2022).
[60] J. Gray, QUIMB: A PYTHON package for quantum information and many-body calculations, J. Open Source Software **3**, 819 (2018).
[61] M. Ostmann, M. Marcuzzi, J. Minář, and I. Lesanovsky, Synthetic lattices, flat bands and localization in Rydberg quantum simulators, Quantum Sci. Technol. **4**, 02LT01 (2019).
[62] S. Moudgalya and O. I. Motrunich, Hilbert space fragmentation and commutant algebras, Phys. Rev. X **12**, 011050 (2022).
[63] S. Moudgalya, B. A. Bernevig, and N. Regnault, Quantum many-body scars and Hilbert space fragmentation: A review of exact results, Rep. Prog. Phys. **85**, 086501 (2022).
[64] F. Balducci, A. Gambassi, A. Lerose, A. Scardicchio, and C. Vanoni, Interface dynamics in the two-dimensional quantum Ising model, Phys. Rev. B **107**, 024306 (2023).
[65] G. H. Wannier, Wave functions and effective Hamiltonian for Bloch electrons in an electric field, Phys. Rev. **117**, 432 (1960).
[66] G. H. Wannier, Dynamics of band electrons in electric and magnetic fields, Rev. Mod. Phys. **34**, 645 (1962).
[67] F. Liu, R. Lundgren, P. Titum, G. Pagano, J. Zhang, C. Monroe, and A. V. Gorshkov, Confined quasiparticle dynamics in long-range interacting quantum spin chains, Phys. Rev. Lett. **122**, 150601 (2019).
[68] V. Lienhard, P. Scholl, S. Weber, D. Barredo, S. de Léséleuc, R. Bai, N. Lang, M. Fleischhauer, H. P. Büchler, T. Lahaye, and A. Browaeys, Realization of a density-dependent Peierls phase in a synthetic, spin-orbit coupled Rydberg system, Phys. Rev. X **10**, 021031 (2020).

[69] F. Perciavalle, D. Rossini, T. Haug, O. Morsch, and L. Amico, Controlled flow of excitations in a ring-shaped network of Rydberg atoms, Phys. Rev. A **108**, 023305 (2023).
[70] J. M. Hickey, S. Genway, and J. P. Garrahan, Signatures of many-body localisation in a system without disorder and the relation to a glass transition, J. Stat. Mech. (2016) 054047.
[71] G. H. Fredrickson and H. C. Andersen, Kinetic Ising model of the glass transition, Phys. Rev. Lett. **53**, 1244 (1984).